Available online at www.sciencedirect.com
SCIENCE DIRECT®
Journal of Power Sources 125 (2004) 221–227
JOURNAL OF POWER SOURCES
www.elsevier.com/locate/jpowsour

A simple preparation method for spherical carbons and their anodic performance in lithium secondary batteries

Ou Jung Kwon, Yoon Seok Jung, Ji Hyun Kim, Seung M. Oh*

School of Chemical Engineering and Research Center for Energy Conversion & Storage, Seoul National University, Seoul 151-744, South Korea

Received 4 July 2003; accepted 12 August 2003

Abstract

This work reports a simple preparation method for spherical hard carbons and graphites. The phenolic resin and methylnaphthalene-derived mesophase pitch (MNMP) powders are employed as the precursor for hard carbon and graphite, respectively. The irregular-shaped precursor powders are converted to spherical carbons by first coating with fine-grained fumed silica powder and carbonizing/graphitizing under an argon atmosphere. Two characteristic features are observed in this preparation. First, among the used silica powders, only those having a hydrophobic surface group are effective for the irregular to sphere conversion. Second, the conversion takes place near the glass transition temperature of the resin and the softening point of the pitch, respectively. Based on these observations, an irregular to sphere conversion mechanism has been proposed. The spherical carbon powders exhibit a higher tap density and smaller surface area than those of the irregular-shaped ones, which is an advantageous feature for practical lithium batteries.

Keywords: Lithium secondary batteries; Spherical carbons; Hard carbons; Graphitic carbons; Mesophase pitches

1. Introduction

There are hundreds of commercially available carbons, including natural and artificial graphites, hard carbons, and cokes. All of these carbonaceous materials reversibly react with lithium to some extent and thus their use as the negative electrode in lithium secondary batteries is actively being sought [1–5]. At present, the most successful carbon materials being used as the negative electrode are the graphitized-mesocarbon microbeads (g-MCMB) that are spherical in shape [6]. In general, spherical carbons offer several advantages over other carbon powders of flake or irregular shape in practical lithium cells. Because of their higher tap density, a larger amount of negative electrode material can be loaded in cells such that a higher volumetric energy density can be achieved. In addition, the initial irreversible capacity loss that arises from the formation of a passivation layer on the cabon surface can be minimized due to a smaller surface area inherent from their spherical shape [7]. Finally, mixing and coating in the electrode fabrication process is much easier with spherical powders than with irregular ones.

This study reports a simple preparation method for spherical carbon powders. The carbon powders are prepared by first coating the precursor powders (resin or pitch) with fumed silica and carbonizing/graphitizing in inert atmosphere. The key factor in this preparation is the utilization of fine-grained fumed silica that has a hydrophobic surface functional group. The role of hydrophobic silica and the temperature for irregular to sphere conversion is examined, from which a plausible mechanism for the sphere conversion is proposed. Physical properties of the resulting carbons such as tap density and surface area, and anodic properties in Li secondary cells are also analyzed.

2. Experimental

2.1. Materials

Phenolic resin (glass transition temperature, $T_g = 83\,^{\circ}C$) and methylnaphthalene-derived mesophase pitch (MNMP, softening point $= 227\,^{\circ}C$) powders were used as the precursor for hard carbon and graphite, respectively. A series of fumed silicas named as CAB-O-SIL® were purchased from Cabot Corp. (USA). The fumed silicas have

* Corresponding author. Tel.: +82-2-880-7074; fax: +82-2-872-5755.
E-mail address: seungoh@plaza.snu.ac.kr (S.M. Oh).

0378-7753/$ – see front matter © 2003 Elsevier B.V. All rights reserved.
doi:10.1016/j.jpowsour.2003.08.012

three-dimensional, chain-like aggregates of approximately 0.2 to 0.3 μm in size. As the particle size of fumed silica is much smaller than that (10 to 15 μm) of the precursor powders, the fumed silica is readily coated on the surface of precursor powders by simple mixing. For the preparation of spherical hard carbons, the phenolic resin powder was first mixed with CAB-O-SIL® TS-530 fumed silica. The silica-coated resin powder was then heat-treated under an argon atmosphere from 25 to 1000 °C with a heating rate of 10 °C min^{-1}, followed by an additional heating at 1000 °C for 1 h. After the carbonization, the silica was removed by treating with 48% aqueous hydrofluoric acid. For the preparation of spherical graphite, the silica (TS-530)-coated MNMP powder was heated at 300 °C for 1 h under an argon atmosphere. The irregular-shaped MNMP powder was converted to a sphere-shape at this stage. The resulting silica-coated spherical MNMP powder was oxidative stabilized at 270 °C for 15 min in air and then carbonized by heating at 1000 °C for 1 h under argon. After removing the silica component, the resulting carbon was further graphitized by heating at 2550 °C for 30 min under argon.

The powder morphology was examined by scanning electron microscopy (SEM; Model JSM-840A, JEOL) and the Si line analysis was made with an energy dispersive X-ray spectrometer (EDS, Oxford Instruments). The tap density was estimated according to the *ASTM* No. B527-93. The surface area was calculated from the N_2 adsorption isotherms (Micrometrics ASAP20-10) using Brunauer, Emmett, and Teller (BET) method.

2.2. Electrochemical measurements

The galvanostatic charge–discharge and electrochemical voltage spectroscopy (EVS) measurements were made in a beaker-type three-electrode cell, in which lithium metal foil was used for both the counter and reference electrodes. The electrolyte was a mixture of ethylene carbonate (EC) and diethyl carbonate (DEC) (1:1 volume ratio) which contained 1.0 M $LiPF_6$. For the preparation of carbon electrodes, a mixture of carbon powder and poly(vinylidene fluoride) (PVdF) (90:10 weight ratio) was coated on a piece of copper foil (1 cm × 1 cm). The moulded carbon electrode was then dried at 120 °C under vacuum for 12 h. The electrode thickness was controlled to be about 100 μm. For the galvanostatic charge–discharge cycling, a gravimetric current density of 50 mA g^{-1} was applied and the potential cut-off was fixed at 0.0 and 2.0 V (versus Li/Li^+). For the EVS measurement, an EG&G M362 scanning potentiostat/galvanostat and a programmable potential source were combined in order to control the applied potential step. The potential step (10 mV) was started from the open-circuit potential of the fresh cell and the sequential step was applied after the current decayed down to the threshold current ($I_{threshold}$ = 0.02 mA). All the electrochemical experiments were carried out at ambient temperature in a glove box filled with argon.

3. Results and discussion

3.1. Preparation of spherical carbons

SEM images of phenolic resin and MNMP powder that were used as the precursors are shown in Fig. 1(a) and (b). Both are irregular in shape with an average particle size of 15 and 12 μm, respectively. A carbonization of phenolic resin at 1000 °C under an argon atmosphere without silica coating produced a lump-shaped carbon, indicative of the evolution of a massive inter-particle cohesion. Surprisingly, however, when the carbonization was carried out after the resin powder was coated with fine-grained fumed silica (CAB-O-SIL®TS-530), the resulting carbon exhibited a spherical shape with an average particle size of 9.7 μm (Fig. 1(c)). Rather curiously, when CAB-O-SIL® M-5 fumed silica was used instead of CAB-O-SIL® TS-530, the resulting carbon formed a lump. TS-530 and M-5 differ only in the surface functional group. The surface of M-5 is covered with hydroxyl groups, whereas it is replaced by trimethylsilyl ($–OSi(CH_3)_3$) groups on the surface of TS-530. It is thus seemingly that the surface functional group of silica is the key factor in controlling the carbon shape; either lump or sphere. Similar results were observed with the methylnaphthalene-derived mesophase pitch (MNMP). The precursor pitch particles are irregular in shape like the phenolic resin (Fig. 1(b)). Carbonization either without silica coating or with M-5 coating produced a lump-shaped carbon, but a spherical carbon with TS-530 coating. An electron micrograph of MNMP-derived spherical carbon is presented in Fig. 1(d).

Cross-sectional electron micrographs and energy dispersive X-ray spectroscopy (EDS) results for a carbon sphere are shown in Fig. 2. The carbon sphere was analyzed before the hydrofluoric acid treatment. As shown, the intensity of the Si signal is much higher at the periphery than in the inside. It is thus very likely that the silica component affects only the surface properties of precursor particles, which eventually plays a key role in the irregular to sphere conversion.

In order to examine the temperature range where the precursor powders transform to a spherical shape, a control experiment was made in which the silica (TS-530)-coated precursor powders were heat-treated over a wide temperature range. When the silica-coated phenolic resin was heated at 80 °C (below T_g of the resin), the initial irregular morphology was sustained. When heated at higher temperature than T_g, however, the resin powder transformed to a spherical shape. It is thus apparent that the onset temperature for the irregular to sphere transformation is near the glass transition temperature of the resin. In the case of silica-coated MNMP, the onset temperature appears to be the softening point (227 °C) of the pitch. That is, the pitch powder maintains its irregular morphology below the softening point, but a spherical shape above it.

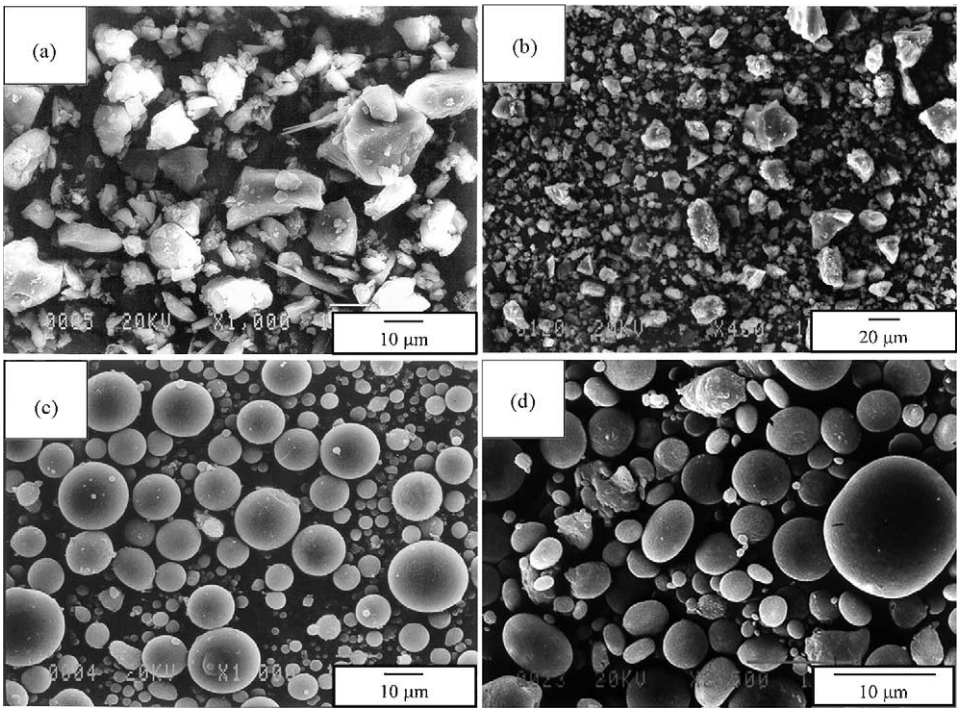

Fig. 1. Electron micrographs of precursor and spherical carbon powders: (a) phenolic resin powder; (b) MNMP powder; (c) phenolic resin-derived spherical carbon; (d) MNMP-derived spherical carbon.

The mechanism along which the silica-coated precursor powders transform from an irregular to spherical morphology is given below. Above the T_g of the resin or softening point of the pitch, the constituent molecules carry a fluid-like character with active segmental motions. Under these circumstances, as the precursor particles are in intimate contact with the silica powder, some mixing or wetting takes place on the surface of precursor particles as the $–OSi(CH_3)_3$ group on the silica surface has a high affinity for the hydrophobic resin or pitch constituents. The net result will be a reduction in the surface energy of the precursor particles so as to discourage inter-particle coalescence. Individual isolated precursor particles then transform to spheres to minimize further the surface energy. The precursor powders that are once converted to a spherical shape at the onset temperature are then carbonized to be spherical carbons upon a continued heating up to 1000 °C. In the absence of silica, however, the precursor powders have a relatively higher surface energy due to the lack of hydrophobic interaction, thereby the precursor particles tend to coalesce to minimize their surface energy. As a result, lump-shaped carbons are produced upon a continued carbonization. The same situation prevails with the M-5 silica coating because the hydrophilic hydroxyl group on the surface of M-5 does not interact with the hydrophobic resin or the pitch surface. It may be proposed that the fine-grained silica acts as a physical barrier to prevent inter-particle cohesion. This possibility can, however, be discarded because the M-5 coating produces a lump-shaped carbon even if the silica is uniformly coated on the precursor powders.

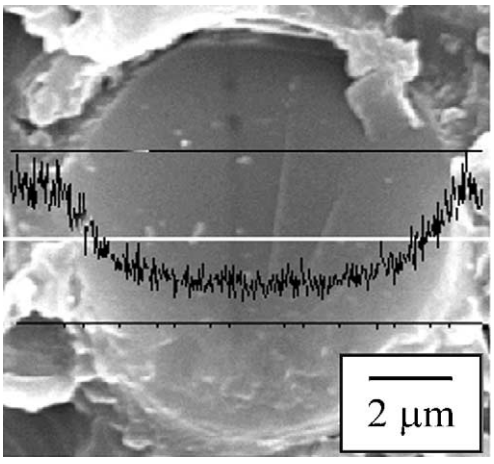

Fig. 2. Electron micrographs of cross-section of a resin-derived carbon sphere and line analysis for Si. The carbon sphere was moulded into epoxy resin and cut using a microtome. Line scan for Si Kα was made along the white line. Note that the silica component has not been removed.

3.2. Anodic properties of spherical carbons

The tap density and specific surface area of spherical carbons are listed in Table 1. For comparison, the results obtained with the pulverized hard carbon that is derived from the lump-shaped one is provided along with those of graphitized mesocarbon microbead (g-MCMB 10-28) and Brazilian graphite (BG). The tap density of spherical hard carbon ($0.9\,g\,ml^{-1}$) is higher than that of the pulverized counterpart

Table 1
Powder and electrochemical properties of hard carbons and graphitic carbons

	Tap density ($g\,ml^{-1}$)	Surface area ($m^2\,g^{-1}$)	First discharge capacity ($mAh\,g^{-1}$)	First coulombic efficiency (%)
Hard carbons				
Pulverized[a]	0.57	446	460	56.0
Spherical	0.9	4.0	480	67.0
Graphitic carbons				
BG[b]	0.67	8.0	360	75.2
g-MCMB 10-28[c]	1.41	2.5	305	89.1
SAG[d]	1.61	1.9	292	91.5

[a] Obtained by pulverizing lump-shaped hard carbon that is prepared without silica coating.
[b] Brazillian graphite, a flake-shaped natural graphite.
[c] Graphitized mesocarbon microbeads (from Osaka Gas Co., average particle diameter = 10 μm, graphitization temperature = 2800 °C).
[d] Spherical artificial graphite prepared from MNMP (graphitization temperature = 2550 °C).

($0.57\,g\,ml^{-1}$). The MNMP-derived spherical graphite (designated as spherical artificial graphite, SAG) exhibits a higher tap density ($1.61\,g\,ml^{-1}$) than that of Brazillian graphite of flake shape ($0.67\,g\,ml^{-1}$), which is even higher than that of g-MCMB 10-28 that carries a similar spherical shape ($1.41\,g\,ml^{-1}$). When the tap density is compared for two types of spherical carbons, the graphitic forms show a higher value than that of hard carbons due to their higher gravimetric density. The spherical hard carbon and graphites carry a smaller surface area (1.9 to $4.0\,m^2\,g^{-1}$) than that of pulverized hard carbon ($446\,m^2\,g^{-1}$) or flake-shaped BG ($8.0\,m^2\,g^{-1}$).

The first galvanostatic charge–discharge potential profile of the resin-derived spherical carbon is shown in Fig. 3. The curve shows different slopes at three potential regions, which manifests the presence of at least three different Li^+ storage sites in this carbon. In the earlier stage, the discharge potential appears as a plateau (span I, 0 to 0.12 V), then a sloping curve (span II, 0.12 to 0.8 V), and finally another sloped curve (span III, above 0.8 V). This is one of the characteristic features of hard carbons that are prepared from cross-linked polymeric precursors or isotropic pitches [8–12]. From this, the resin-derived spherical carbon can be categorized as hard carbon. The cycling performance of spherical hard carbon is given in Fig. 4. In the first cycle, the charging and discharging capacity amounts to 700 and $480\,mAh\,g^{-1}$, respectively, from which a coulombic efficiency of 67% is calculated. From the second cycle, however, the coulombic efficiency amounts to >99% with a discharge capacity of $450\,mAh\,g^{-1}$. In the case of pulverized hard carbon, the first discharge capacity is comparable with that of spherical hard carbon, but the first coulombic efficiency is slightly lower (Table 1).

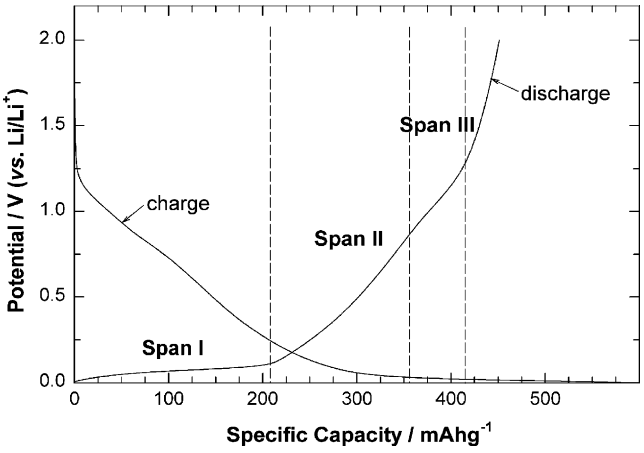

Fig. 3. First galvanostatic charge–discharge potential profile of phenolic resin-derived spherical carbon.

The major problem encountered in using either hard carbons or graphitic carbons as the anode in lithium secondary batteries is the irreversible reactions that inevitably occur during the first charging period of cell operation [1,2]. A surface layer, known as the solid electrolyte interface (SEI), forms as a result of electrolyte decomposition and subsequent deposition of reaction products. Many previous studies have confirmed that the extent of SEI formation is proportional to the surface area of carbon [2,13–19]. In the case of hard carbons, however, the irreversible storage (trapping) of Li^+ ions at voids or cavity sites that are highly populated in this type of carbon has been proposed to be an additional factor in lowering the coulombic efficiency [20]. In the present work, it is clear that the irreversible capacity loss caused by SEI formation prevails in the first cycle in both the pulverized and spherical hard carbons. Given that the first coulombic efficiency of pulverized hard carbon (56%) is not significantly lower than that of the spherical form (67%), even if its surface area is two orders of magnitude larger than the spherical one, the irreversible capacity loss caused by Li^+ trapping appears dominant over the SEI formation in these hard carbons.

The first galvanostatic charge–discharge potential profile of MNMP-derived spherical carbon is displayed in Fig. 5 along with those for g-MCMB 10-28 and BG. The stage phenomenon appearing at 0.0–0.3 V (versus Li/Li^+) in both the charging and discharging curves, which is also apparent in g-MCMB 10-28 and BG, indicates that this carbon is a graphite [21–25]. The anodic performance of SAG is compared with that of g-MCMB 10-28 and BG in Fig. 5, and the

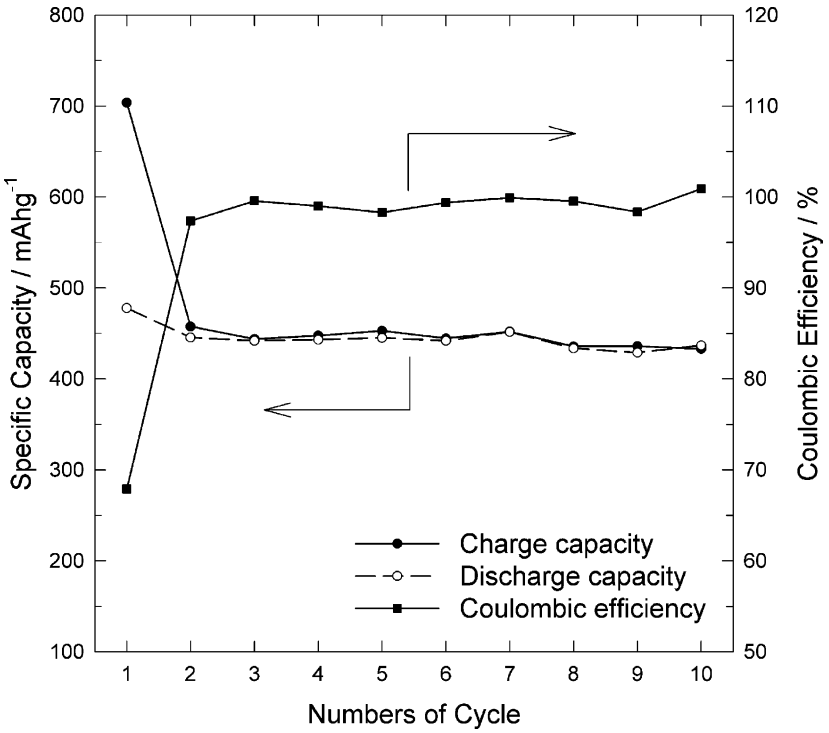

Fig. 4. Cycle performance of spherical hard carbon. (Galvanostatic charge–discharge cycling condition is provided in the Section 2.)

relevant data are listed in Table 1. Here, two features are apparent. First, the SEI formation reaction occurring at 0.6 to 0.9 V is roughly proportional to the surface area of graphitic materials, indicating that the irreversible capacity loss associated with SEI formation is dominant over Li^+ trapping. This is consistent with the literature in which it is claimed that Li^+ trapping is not serious in highly graphitized materials [20]. Second, the first discharge capacity differs for three graphitic materials. The SAG delivers a discharge capacity of 292 mAh g^{-1} in the first cycle, which is smaller than that of BG or g-MCMB 10-28. This may be attributed to the difference in the degree of graphitization of the three graphites. Clearly, BG, the natural graphite, possesses the highest degree of graphitization among the three materials. The graphitization temperature for SAG is 2550 °C and is lower than that of g-MCMB 10-28 (2800 °C), thereby the extent

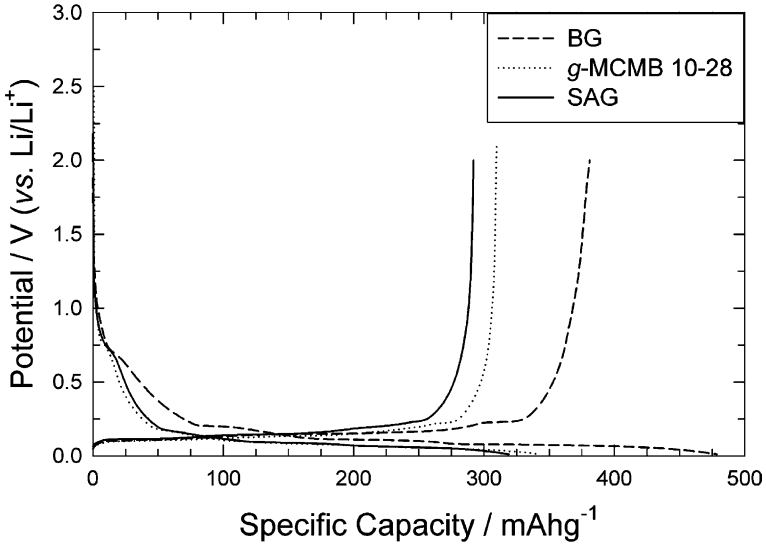

Fig. 5. First galvanostatic charge–discharge potential profile of MNMP-derived spherical carbon. Profiles for Brazillian graphite (BG) and graphitized mesocarbon microbead g-MCMB 10-28 are provided for comparison.

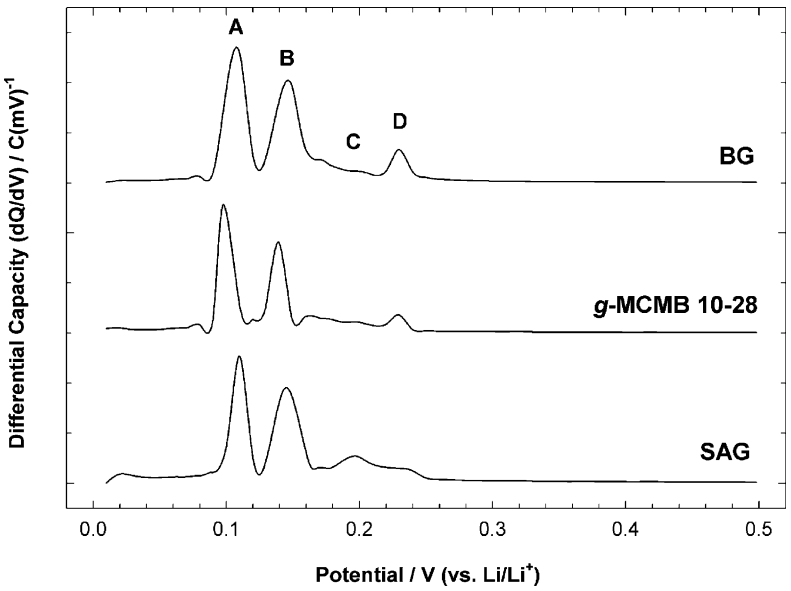

Fig. 6. Electrochemical voltage spectroscopy (EVS) profiles obtained in first discharging period. Note the change in intensity and position of the four separable peaks that are related with stage phenomenon in graphitic materials.

of graphitization appears to be lower in the case of SAG. The extent of graphitization in the three graphites can be more clearly compared by examining the discharging EVS profiles (Fig. 6). All the graphitic materials give at least four separable peaks in the differential discharge capacity profiles, which are related with the stage phenomenon [21–25]. In a previous study [26], the extent of graphitization for needle cokes was evaluated by changing the graphitization temperature. By increasing the graphitization temperature from 2000 to 3000 °C, the needle cokes became more graphitized. The most apparent feature with an increase in the degree of graphitization is the variation in the intensity and position of the differential capacity peaks in the EVS profiles. In detail, the peak labeled *D* (a coexistence of stage 4/1′ (dilute stage 1)) steadily grows with increasing graphitization, whereas the peak labeled *C* (a coexistence of stage 2L (liquid-like stage 2)/3 or 3/4) decreases in intensity along with a negative peak shift. Based on this, the extent of graphitization is compared for the three. As shown in Fig. 6, SAG exhibits the weakest peak *D*, but the most intense peak *C* among the three; this is indicative of the lowest degree of graphitization. In the other extreme, BG gives the highest peak *D*, but the lowest peak *C*. The peak labeled *C* is superimposed with the peak *B*, and thereby appears as a shoulder in the EVS profile. Judging from the peak intensity and position of peaks labeled *C* and *D*, the degree of graphitization in g-MCMB 10-28 appears to be intermediate between that of SAG and BG.

4. Conclusions

Spherical hard carbons and graphites have been prepared by coating the precursor powders with fumed silica powder, followed by a heat treatment. Among the chosen fumed silicas, only those having a hydrophobic surface functional group are effective in converting the irregular-shaped precursor powders to spherical carbons. The irregular to sphere conversion takes place near the glass transition temperature of the resin and the softening point of MNMP, respectively. The underlying role of hydrophobic silica is to lower the surface energy of the precursor particles which eventually suppresses the inter-particle coalescence. The resulting spherical carbons carry a higher tap density and a smaller surface area compared with those of the pulverized carbon and flake-shaped natural graphite. Due to the smaller surface area of the spherical artificial graphite, the first irreversible capacity is smaller than that of BG that carries a larger surface area. The degree of graphitization in SAG is, however, slightly lower than those of BG or g-MCMB 10-28 due to a lower graphitization temperature.

Acknowledgements

This work has been supported by KOSEF through Research Center for Energy Conversion and Storage.

References

[1] J.R. Dahn, A.K. Sleigh, H. Shi, J.N. Reimers, Q. Zhong, Electrochim. Acta 38 (1993) 1179.
[2] M. Winter, J.O. Besenhard, M.E. Spahr, P. Novák, Adv. Mater. 10 (1998) 725.
[3] S. Flandrois, B. Simon, Carbon 37 (1999) 165.
[4] M. Endo, C. Kim, K. Nishimura, T. Fujino, K. Miyashita, Carbon 38 (2000) 183.
[5] E. Buiel, J.R. Dahn, Electrochim. Acta 45 (1999) 121.

[6] R. Alcántara, F.J. Fernández, P. Lavela, J.L. Tirado, J.M. Jiménez Mateos, C. Gómez de Salazar, R. Stoyanova, B. Zhecheva, Carbon 38 (2000) 1031.
[7] J.O. Besenhard, Handbook of Battery Materials, Lithiated Carbons, WILEY-VCH, Weinheim, 1999, pp. 383–418.
[8] J.R. Dahn, T. Zheng, Y. Liu, J.S. Xue, Science 270 (1995) 590.
[9] Y. Liu, J.S. Xue, T. Zheng, J.R. Dahn, Carbon 34 (1996) 193.
[10] N. Takami, A. Satoh, T. Ohsaki, M. Kanda, Electrochim. Acta 42 (1997) 2537.
[11] Z. Ogumi, M. Inaba, Bull. Chem. Soc. Jpn. 71 (1998) 521.
[12] C.W. Park, S.H. Yoon, S.I. Lee, S.M. Oh, Carbon 38 (2000) 995.
[13] A.N. Dey, B.P. Sullivan, J. Electrochem. Soc. 117 (1970) 222.
[14] R. Fong, U. von Sacken, J.R. Dahn, J. Electrochem. Soc. 137 (1990) 2009.
[15] Z.X. Shu, R.S. McMillan, J.J. Murray, J. Electrochem. Soc. 140 (1993) 922.
[16] D. Aurbach, Y. Ein-Eli, O. Chusid, Y. Cameli, M. Babai, Y. Yamin, J. Electrochem. Soc. 141 (1994) 603.
[17] J.O. Besenhard, M. Winter, J. Yang, W. Biberacher, J. Power Sources 54 (1995) 228.
[18] B. Buiel, J.R. Dahn, J. Electrochem. Soc. 144 (1998) 1977.
[19] H. Fujimoto, A. Mabuchi, K. Tokumitsu, T. Kasuh, J. Power Sources 54 (1995) 440.
[20] K. Guerin, A. Fevrier-Bouvier, S. Flandrois, B. Simon, F. Biensan, Electrochim. Acta 45 (2000) 1607.
[21] T. Ohzuku, Y. Iwasashi, K. Sawai, J. Electrochem. Soc. 140 (1993) 2490.
[22] J.R. Dahn, R. Fong, M.J. Spoon, Phys. Rev. B 42 (1990) 6424.
[23] J.R. Dahn, Phys. Rev. B 44 (1995) 9170.
[24] N. Daumas, A. Herold, C.R. Acad. Sci. Paris 268 (1969) C373.
[25] K.C. Woo, W.A. Kamitakahara, D.P. DiVincenzo, D.S. Robinson, H. Mertwoy, J.W. Milliken, J.E. Fischer, Phys. Rev. Lett. 50 (1983) 182.
[26] C.W. Park, S.H. Yoon, S.M. Oh, Carbon 38 (2000) 1261.